Crisis, unstable dimension variability, and bifurcations in a system with high-dimensional phase space: Coupled sine circle maps

Alaka Das* and Neelima Gupte
Department of Physics, Indian Institute of Technology Madras, Chennai 600036, India
(Received 7 August 2012; revised manuscript received 22 January 2013; published 8 April 2013)

The phenomenon of crisis in systems evolving in high-dimensional phase space can show unexpected and interesting features. We study this phenomenon in the context of a system of coupled sine circle maps. We establish that the origins of this crisis lie in a tangent bifurcation in high dimensions, and identify the routes that lead to the crisis. Interestingly, multiple routes to crisis are seen depending on the initial conditions of the system, due to the high dimensionality of the space in which the system evolves. The statistical behavior seen in the phase diagram of the system is also seen to change due to the dynamical phenomenon of crisis, which leads to transitions from nonspreading to spreading behavior across an infection line in the phase diagram. Unstable dimension variability is seen in the neighborhood of the infection line. We characterize this crisis and unstable dimension variability using dynamical characterizers, such as finite-time Lyapunov exponents and their distributions. The phase diagram also contains regimes of spatiotemporal intermittency and spatial intermittency, where the statistical quantities scale as power laws. We discuss the signatures of these regimes in the dynamic characterizers, and correlate them with the statistical characterizers and bifurcation behavior. We find that it is necessary to look at both types of correlators together to build up an accurate picture of the behavior of the system.

DOI: 10.1103/PhysRevE.87.042906 PACS number(s): 05.45.−a

I. INTRODUCTION

The phenomenon of crisis is commonly observed in dissipative systems with chaotic dynamics, and is manifested by a sudden discontinuous change in a chaotic attractor as a system parameter is varied [1,2]. The discontinuous changes are typically of three types: as a system parameter passes through a critical value, either a chaotic attractor is destroyed, or the size of the chaotic attractor in phase space suddenly increases, or two or more chaotic attractors merge to form one chaotic attractor. The inverse of these processes can also occur, if the parameter change takes place in the reverse direction. The three major types of crises associated with these changes are called the boundary crises (associated with attractor creation or destruction), the interior crises, associated with sudden changes in shape and size, and the symmetry restoring or breaking crises, in which attractors merge or split. The phenomenon is often associated with intermittency of a type called crisis induced intermittency, and also with unstable dimension variability [3,4], which occurs when a chaotic attractor contains embedded periodic orbits with different numbers of expanding directions leading to Lyapunov exponents which fluctuate around zero. The phenomenon of crisis, its effects, and its connection with bifurcations are well studied in the context of low-dimensional dynamical systems [1–4]. However, there are very few studies of crisis and its consequences in the context of systems with high-dimensional phase space. In the case of spatially extended systems, the crisis, a dynamical phenomenon, can have consequences for the statistical as well as the dynamical behavior of the system. The bifurcation behavior of the system, as well as phenomena such as unstable dimension variability, can have important implications for the behavior of the extended system. On the other hand, the existence of Milnor attractors and multiple basins of attraction in the extended system can lend unexpected features to the consequences of the crisis. Model studies are important for understanding these aspects. This paper attempts to study some of the features of the crisis in the context of a simple model system, a lattice of coupled sine circle maps.

The coupled sine circle map lattice is known to model the mode-locking behavior seen in coupled oscillators, Josephson junction arrays, etc. The phase diagram of this system is known to exhibit a rich diversity of dynamic behavior. In particular, this system shows transitions from nonspreading to spreading transitions, across an infection line, with the transition from spatial intermittency to spatiotemporal intermittency being seen as a special case. Earlier studies indicate that the dynamic origins of this transition lie in a crisis [5] and unstable dimension variability. In this paper we confirm the existence of unstable dimension variability in the system, and study the details of this crisis using dynamic characterizers such as Lyapunov exponents, finite-time Lyapunov exponents, and their distributions. Our studies indicate that the origins of this crisis lie in a tangent bifurcation in high dimensions. We also identify the route that leads to crisis in the system, and find that it depends on the parameter as well as on initial conditions. Thus, there are multiple routes to crisis due to the high dimensionality of the phase space of the system and the presence of Milnor attractors. While this phenomenon has not been extensively studied, we note that multiple coexisting attractors with fractal basin boundaries, as well as crisis induced transitions, have been seen earlier in models of food chains [6,7]. It has been noted that the presence of these features may make these systems highly susceptible to external perturbations and leads to high unpredictability for dynamical behavior. Given that the coupled sine circle map system studied here is a discrete version of the coupled oscillator systems which model the behavior of a vast variety of experimental and natural systems, a similar unpredictability of dynamical behavior would have serious practical consequences.

*Permanent address: Department of Mathematics, Jadavpur University, Kolkata 700032, India.

The statistical behavior of the system has also been extensively studied in earlier work. Special spreading and nonspreading solutions are seen at the boundaries of the synchronized solutions seen above and below the infection line in the phase diagram. These correspond to spatiotemporally intermittent and spatially intermittent solutions, respectively. The statistical signature of these solutions is the power-law behavior of the laminar length distributions with their own characteristic power. We will see that these solutions also contribute their own signatures to the dynamic quantifiers. We correlate these signatures with the bifurcation behavior and statistical behavior of the system. We note that both statistical and dynamical signatures need to be studied together to understand the behavior of the system completely.

We note that the evolution of systems with a large number of degrees of freedom is important in a large variety of contexts, especially those that show pattern formation. Examples of these include fluid systems [8], chemical reactions [9,10], biological systems such as neural networks [11], and phenomena like ventricular fibrillation [12], as well as the formation of coherent structures such as the red spot of Jupiter [13]. Spatio-temporal intermittency and spatial intermittency constitute a very special type of pattern which is observed in many experimental situations such as chemical reactions [14], Rayleigh-Benard and Couette flows [15,16], as well as theoretical models [17,18], and the synchronisation-desynchronisation transitions [19].

It is well known that dynamical system techniques can be of great utility in understanding and characterising such systems [19], and also that the tools required to study such large systems require further development [20]. Our studies provide pointers to the manner in which dynamic characterizers can be of utility in the study of such systems, and can complement the information obtained from the usual statistical characterizers.

II. THE MODEL AND THE PHASE DIAGRAM

We describe the model and the phase diagram in this section. The coupled sine circle map lattice is defined by the evolution equation

$$x_i^{t+1} = (1-\epsilon) f\left(x_i^t\right) + \frac{\epsilon}{2}\left[f\left(x_{i-1}^t\right) + f\left(x_{i+1}^t\right)\right] (\mathrm{mod}\ 1), \quad (1)$$

where i and t are the discrete site and time indices, respectively, $i = 1, \ldots, N$, where N is the number of lattice sites, and ϵ is the strength of coupling between the site i and its two nearest neighbors. The local on-site map, $f(x)$, is the sine circle map, defined as

$$f(x) = x + \Omega - \frac{K}{2\pi}\sin(2\pi x), \quad (2)$$

where K is the strength of nonlinearity and Ω is the winding number of the single sine circle map in the absence of nonlinearity.

The phase diagram of this system is highly sensitive to initial conditions due to the presence of many degrees of freedom. The phase diagram obtained by evolving the model starting from randomly chosen initial conditions is shown in Fig. 1 at the parameter value $K = 1$, for the range $0 \leqslant \Omega \leqslant \frac{1}{2\pi}$, $0 \leqslant \epsilon \leqslant 1$. Periodic boundary conditions have been imposed.

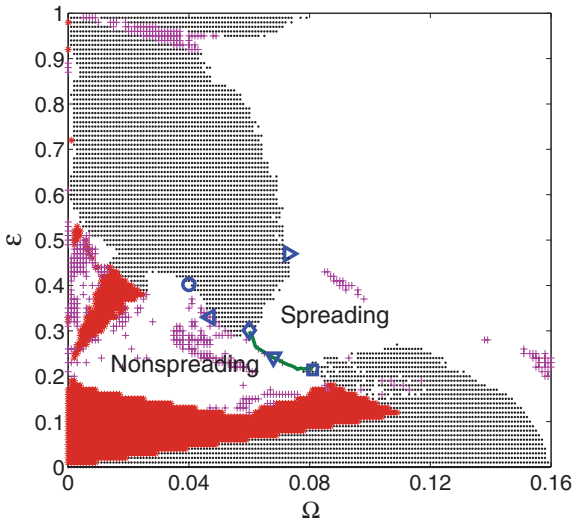

FIG. 1. (Color online) The phase diagram of the coupled sine circle map lattice in Ω-ϵ plane starting from a randomly chosen initial condition with lattice size $L = 200$. Each lattice has been iterated for 5000 iterates after discarding 200 000 iterates. The synchronized fixed point solution is denoted by dots (.), whereas the nonsynchronized solutions fixed in time, and periodic in time with period $T = 15 \times 16$, are marked by star ($\star$) and plus signs (+), respectively. The spreading and nonspreading solutions are separated by the infection line (shown by a solid line). The left end point ($\Omega = 0.060, \epsilon = 0.30$), a point in the middle ($\Omega = 0.068, \epsilon = 0.24$), and the right end point ($\Omega = 0.081$, $\epsilon = 0.21$) of the infection line are marked by a diamond ($\Diamond$), a down triangle ($\triangledown$), and a square ($\square$), respectively. At the point ($\Omega = 0.047$, $\epsilon = 0.3360$) marked with a left triangle ($\triangleleft$), spatial intermittency with period-5 bursts is seen. Spatial intermittency with quasiperiodic bursts is seen at the point ($\Omega = 0.040$, $\epsilon = 0.402$) marked by a circle ($\bigcirc$). Spatiotemporal intermittency is seen at the point marked by a right triangle ($\triangleright$).

A large part of the diagram is occupied by the spatiotemporally fixed point solution (denoted by dots) wherein all the sites converge to the fixed point

$$x^* = \frac{1}{2\pi}\sin^{-1}\left(\frac{2\pi\Omega}{K}\right), \quad (3)$$

which is the same as the fixed point of the single circle map. In addition, the phase diagram also shows solutions which are either nonsynchronized fixed points (indicated by plus signs)

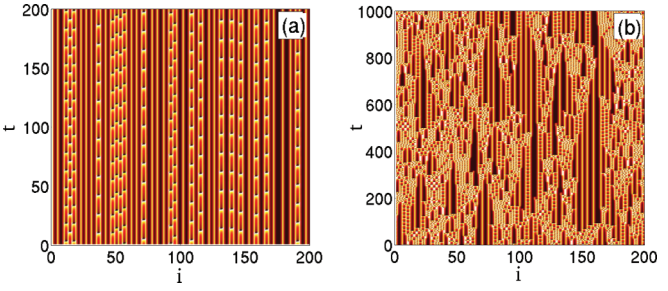

FIG. 2. (Color online) (a) Space-time plots of typical nonspreading solutions at (a) $\Omega = 0.065$ and $\epsilon = 0.252$. The bursts are periodic and have period 15×16. (b) A typical spreading solution at $\Omega = 0.065$ and $\epsilon = 0.254$.

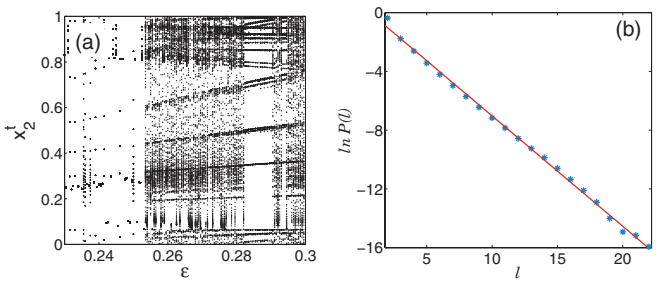

FIG. 3. (Color online) The bifurcation diagram of the coupled map lattice. A typical site x_i^t is plotted over 500 time steps as a function of the coupling strength ϵ in the region near the middle of the infection line, at $\Omega = 0.065$. The lattice size is $L = 200$. A transient of 500 000 iterates has been discarded. (b) The semilog plot of laminar length distribution at $\Omega = 0.068$ and $\epsilon = 0.244$. The distribution shows exponential fit $P(l) = ae^{-bl}$ with $b = 0.7512 \pm 0.0172$ and $a = 0.4813 \pm 0.2313$. The root-mean-square error is 0.2281 and R^2 value is 0.9977.

or nonsynchronized and periodic (denoted by stars) in time [21]. The periodic solution shown here has temporal period $T = 15 \times 16$.

The phase diagram is divided into two distinct regimes, separated by a line, the infection line, indicated by a solid line in Fig. 1. A spreading regime where the burst states can infect their neighboring laminar states and spread through the lattice can be seen above the infection line [5,22,23]. (Here, the sites which relax to the fixed point solution $x^\star$ are identified as the laminar sites.) This is in contrast to the nonspreading regime seen below the infection line, where the random initial conditions die down to bursts which are localized, and do not infect their neighboring laminar states. The space-time plots of typical nonspreading solutions are shown in Fig. 2(a), and those of spreading solutions are seen in Fig. 2(b).

Earlier results indicate that the change in the behavior of the solutions from noninfecting to infecting is due to a dynamical phenomenon, the existence of a crisis in the system at the parameter values corresponding to the infection line [5]. A crisis is described as a discontinuous change in the system attractor for a small change in a parameter value of the system [1]. Such a phenomenon is observed in our model, when we increase the coupling strength ϵ at a given Ω in the vicinity of the infection line, in a direction in which the infection line is crossed. The bifurcation diagram of Fig. 3(a) shows this behavior. Here, a typical variable x_i^t is plotted over 500 time steps, as a function of the coupling strength ϵ at the value $\Omega = 0.065$. The bifurcation diagram shows that the crisis appears at $\epsilon = 0.255$ for $\Omega = 0.065$ where the attractor widens from a periodic trajectory to a chaotic structure which accesses the entire range from zero to 1. The value of the critical parameter ϵ_c exactly matches with the value of ϵ, where a vertical line crosses the infection line at $\Omega = 0.065$ in the phase diagram, indicating a clear connection between the spreading transition seen in the space-time plots and the crisis seen in the bifurcation diagram.

We characterize this crisis further in the next section, and study the bifurcation behavior which gives rise to the crisis. The phenomena associated with the crisis can be most clearly seen in the region near the midpoint of the infection line. We note that the behavior of the solutions is different at different points along the infection line, but for each kind of solution, the crisis occurs via a tangent bifurcation. We study the behavior for different regimes using dynamical characterizers, and identify the route to crisis. We find that the route to crisis is initial condition dependent, due to the high dimensionality of the system. There are thus multiple routes to crisis in this system.

It is also pertinent to discuss the behavior of the statistical characterizers at this point. The behavior of the distribution of laminar lengths is an important statistical characterizer of intermittency. The length of the laminar state before being interrupted by a chaotic burst is calculated at different time steps and averaged over several different initial conditions. In both the nonspreading and spreading regimes, at the bifurcation boundary of the synchronized solutions, the distribution of laminar length is seen to follow power-law behavior [22], as we will see in the next section. In contrast, the distribution falls off exponentially in the vicinity of the infection line as is illustrated in Fig. 3(b) for $\Omega = 0.068$, due to the presence of infecting and noninfecting bursts. Hence no scaling behavior is seen in the crossover region near to the boundary. Similar behavior is seen for $\Omega = 0.065$ as well.

Further, special spreading and nonspreading solutions are seen above and below the infection line at the boundaries of the synchronized solutions. Statistical characterizers, such as exponents, can be used to characterize these solutions. The special solutions are associated with power-law behavior and exponents in the distribution of laminar lengths, whereas other solutions do not show this power-law behavior. These exponents correspond to spatiotemporal intermittency of the directed percolation type in the spreading region [24,25], and to spatial intermittency which does not belong to the directed percolation class in the nonspreading region. We correlate these statistical characterizers and exponents with the signatures of these solutions seen in the dynamical characterizers, viz. the Lyapunov exponents and their distributions, in later sections.

TABLE I. Periods of the solution for different values of coupling strength ϵ starting from ten randomly chosen initial conditions at $\Omega = 0.065$ for lattice size $L = 50$.

ϵ	I	II	III	IV	V	VI	VII	VIII	IX	X
0.251	15×16	16	16	16	16	16	16	15×16	15×16	16
0.252	15×16	15×16	15×16	15×16	15×16	15×16	15×16	15×16	15×16	15
0.253	15	15	15×31	15	15×31	15	15×31	15×31	15×31	1
0.254	15	1	15	15	15	1	crisis	15	15	15
0.255	crisis	crisis	crisis	crisis	crisis	crisis	crisis	crisis	1	crisis

TABLE II. Periods of the solution for different values of coupling strength ϵ starting from ten randomly chosen initial conditions at $\Omega = 0.068$ for lattice size $L = 200$.

ϵ	I	II	III	IV	V	VI
0.238	$2^4 \times 5 \times 17 \times 23$	$2 \times 5 \times 19 \times 23$	$2^3 \times 5 \times 17$	$2 \times 3^2 \times 5 \times 17$	$5 \times 17 \times 37$	$2 \times 3^2 \times 5 \times 17$
0.239	$2^4 \times 5$	$2^4 \times 5 \times 13$	$2^4 \times 5$	$2^4 \times 3^2 \times 5$	$2^4 \times 5 \times 37$	$2^4 \times 5 \times 11 \times 37$
0.240	$2^4 \times 5$	$2^4 \times 5$	$2^4 \times 3 \times 5 \times 43 \times 113$	$2^4 \times 5$	$2^4 \times 3 \times 5 \times 13$	$2^4 \times 5$
0.241	2^4	2^4	2^4	2^4	2^4	2^4
0.242	15×16	15×16	crisis	crisis	crisis	15×16
0.243	crisis	crisis	crisis	crisis	crisis	crisis

III. THE CRISIS AT THE INFECTION LINE

The phenomena associated with the crisis can be most clearly seen in the region near the midpoint of the infection line. We discuss the behavior seen at the points $\Omega = 0.065$ and $\Omega = 0.068$ in this region. Similar behavior is seen at both points. The most important phenomena seen here are the presence of unstable dimension variability, and the existence of multiple routes to chaos.

A. Multiple routes to crisis

In the nonspreading regime, observed below the infection line, all sites evolve periodically in time. These periodic attractors are Milnor attractors [26], which are globally stable but locally unstable. Therefore an arbitrary small perturbation to an orbit at a Milnor attractor can kick the orbit away from it to a different attractor, even though a finite measure of initial conditions is attracted to the attractor by temporal evolution. Such attractors are very common in high-dimensional systems. The period of the attractor in the precrisis region also depends on the initial conditions. The periods of the attractor before crisis for different initial conditions for lattice size $L = 50$ are listed in Table I for $\Omega = 0.065$ and for $L = 200$ are listed in Table II for $\Omega = 0.068$. The period of the system is obtained by calculating the least common multiplier of the periods of all sites. We use the fast Fourier transform method to find the periods of all sites. It is clear that there are multiple routes to crisis, depending on the initial conditions.

We find temporal periods 1, 15, 16, 15×16, 15×31, $15 \times 16 \times 31$ for $\Omega = 0.065$ in the vicinity of the infection line just before the crisis for the lattice size $L = 50$. The temporal fixed point solution appears just before the crisis for all initial conditions. The route to crisis changes for a larger lattice size. Periodic solutions with large periods can be seen in the system with larger numbers of degrees of freedom. The period of the solution in the precrisis region just before the crisis also depends on the value of the parameter Ω, as Ω corresponds to the frequency of the single circle map. This has been illustrated in Table III which lists the last period seen before crisis at different values of Ω. For values of $\Omega = 0.068$ and above, the period-16 solution become unstable after the crisis [27].

To study the stability of these periodic orbits, we calculate the Floquet multiplier of the periodic solution (i.e., the eigenvalues of the linear stability matrix corresponding to a given period) before and after the crisis. The critical value ϵ_c is obtained by noting the value of ϵ at which the largest Floquet multiplier crosses the unit circle. The values of ϵ_c as a function of Ω are plotted by a solid line in the phase diagram (Fig. 1). We find that the largest eigenvalue always crosses the unit circle through the positive real axis. This implies that the transition from the temporal periodic solution to spatiotemporal chaos is via a tangent bifurcation. We list the Floquet multipliers of orbits of various periods for $\Omega = 0.068$ for different values of the parameter ϵ in Table IV. It can be seen that 12 Floquet multipliers of period 16 cross the unit circle at $\epsilon = 0.242$, consistent with the route described earlier, and the existence of a high-dimensional tangent bifurcation.

The nature of the bifurcation can be further confirmed by looking at the return map. The sixteenth iterate of a typical site is plotted against the site before crisis [Figs. 4(a), 4(b)] and after crisis [Figs. 4(c), 4(d)] for $\Omega = 0.068$. In the precrisis region this particular site has temporal period 1 for $\epsilon = 0.241$ although the period of the system is 16. The fixed point solution of the site is indicated by a star in the figure. The expanded view near the fixed point (right column in Fig. 4) shows that the function is tangent to the $y = x$ line passing through the fixed point just before the crisis. The function goes up, i.e., away from the fixed point after crisis, due to a tangent bifurcation. Thus, the periodic solution destabilizes to a chaotic solution after a tangent bifurcation at the crisis point. The table of Floquet multipliers at $\Omega = 0.060$ (Table V) also shows that several Floquet multipliers cross one simultaneously at the spreading transition, at $\epsilon = 0.301$. Thus the bifurcation seen here, is also a tangent bifurcation in high dimensions.

B. Crisis: Dynamic characterization and unstable dimension variability

The crisis can be analyzed further, using dynamic characterizers. We use the usual quantifiers of chaos, viz. Lyapunov exponents and finite-time Lyapunov exponents (FTLEs), to quantify the crisis. Here, we examine the distributions of

TABLE III. Periods of the solution for different values of Ω and ϵ starting from one randomly chosen initial condition for lattice size $L = 200$.

Ω	0.062	0.063	0.065	0.066	0.067	0.068	0.069	0.070	0.071	0.072	0.073	0.074
ϵ	0.266	0.261	0.252	0.248	0.245	0.241	0.237	0.234	0.231	0.228	0.225	0.222
Periods	15	15	15×16	15×16	15×16	16	16	16	16	16	16	16

TABLE IV. Floquet multipliers at $\Omega = 0.068$ starting from one randomly chosen initial condition after discarding 210 000 iterates for lattice size $L = 200$.

ϵ	Nature of solution	Number of Floquet multipliers more than 1
0.238	time periodic with period 5×17	0
0.239	time periodic with period $5 \times 16 \times 37$	0
0.240	time periodic with period $5 \times 16 \times 39$	0
0.241	times periodic with period 16	0
0.242	crisis	12 (period-16 Floquet exponent)
0.243	crisis	15 (period-16 Floquet exponent)

finite-time Lyapunov exponents (i.e., finite-time averages of the local stretching rates) at points near the infection line. This is shown in Fig. 5 for $\Omega = 0.065$ and for (a) $\epsilon = 0.251$ (precrisis), and (b) $\epsilon = 0.253$ (postcrisis). There is a change in the distribution from (a) to (b) which shows the histogram at precrisis and postcrisis values. The gap in the histogram before crisis indicates that the distribution of finite-time Lyapunov exponents is discontinuous before the crisis, indicating the presence of localized or nonspreading modes. It becomes continuous above the critical value, indicating the existence of extended or spreading modes. The same signature can be seen in the distribution of the variance of Lyapunov exponents [shown in Figs. 5(e) and 5(f)]. It depicts the variance of the FTLEs at an instant for $\Omega = 0.065$ and at (e) $\epsilon = 0.251$, (f) $\epsilon = 0.253$. The distribution becomes smoother on approaching the critical parameter ϵ_c, the value at which the infection line is crossed, at a fixed Ω. We noticed a significant change in the distribution of difference between

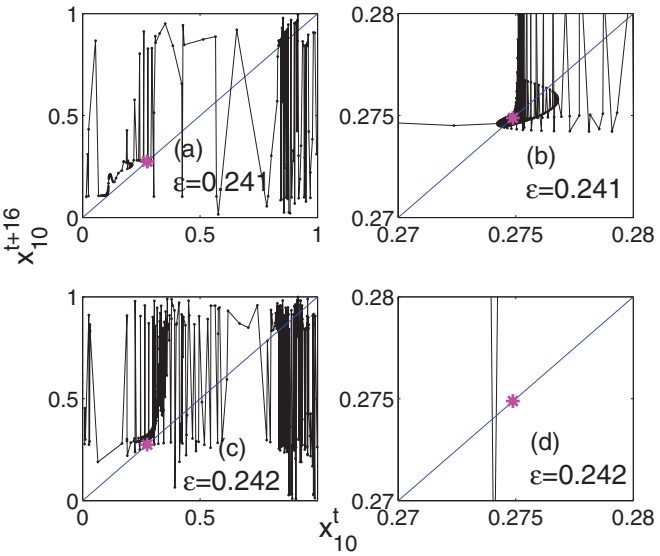

FIG. 4. (Color online) The site x_{10}^{t} is plotted with x_{10}^{t+16} with $\Omega = 0.068$ and for $\epsilon = 0.241$ (top row) and $\epsilon = 0.242$ (bottom row). The right column is the expanded view of the left column.

TABLE V. Floquet multipliers at $\Omega = 0.060$ starting from one randomly chosen initial condition after discarding 210 000 iterates for lattice size $L = 200$.

ϵ	Nature of solution	Number of Floquet multipliers more than 1
0.300	synchronized	0
0.301	crisis	42
0.302	crisis	40
0.303	crisis	45
0.304	synchronized	0
0.305	synchronized	0

two consecutive finite-time Lyapunov exponents [Figs. 5(c) and 5(d)]. The distribution shows a sharp peak near to zero in both cases. The difference in scale of the x axis of Figs. 5(c) and 5(d) should be noted. Figure 5(d) shows that most of the finite-time Lyapunov exponents are not well separated after the transition. However, before the transition the distribution is more spread out, due to the presence of both well separated and not so well separated FTLEs. Similar behavior is seen for $\Omega = 0.068$ [28]. Thus, the distributions of finite-time Lyapunov exponents show the signature of the crisis, where the attractor widens from a periodic trajectory to a chaotic one. More importantly, this system also shows the phenomenon of unstable dimension variability near the crisis. We study this in detail in the subsequent discussion.

Our system shows unstable dimension variability (UDV) in the vicinity of the infection line. This phenomenon occurs when a chaotic attractor contains embedded periodic orbits with different numbers of expanding directions. The existence

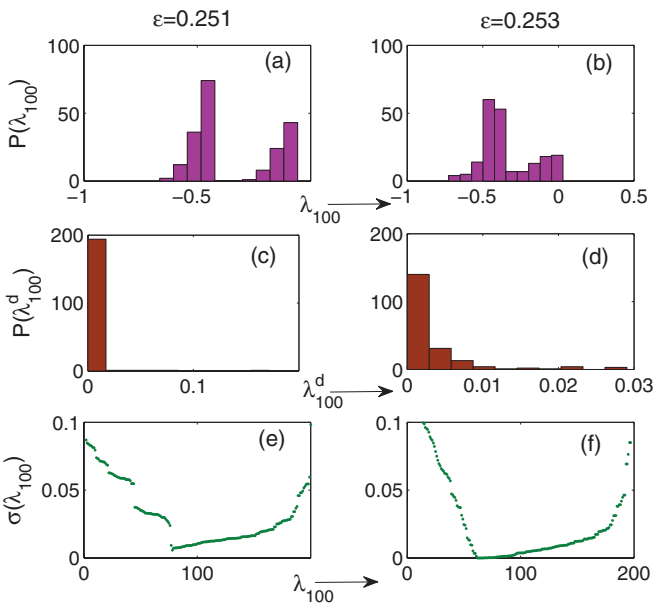

FIG. 5. (Color online) The distribution of 100-time Lyapunov exponents [(a), (b)], the difference between two consecutive 100-time Lyapunov exponents [(c), (d)], and variance of 100-time Lyapunov exponents [(e), (f)] for $\Omega = 0.065$. The left and right columns correspond to the values of ϵ before and after crisis, respectively. Here, lattice size $L = 200$.

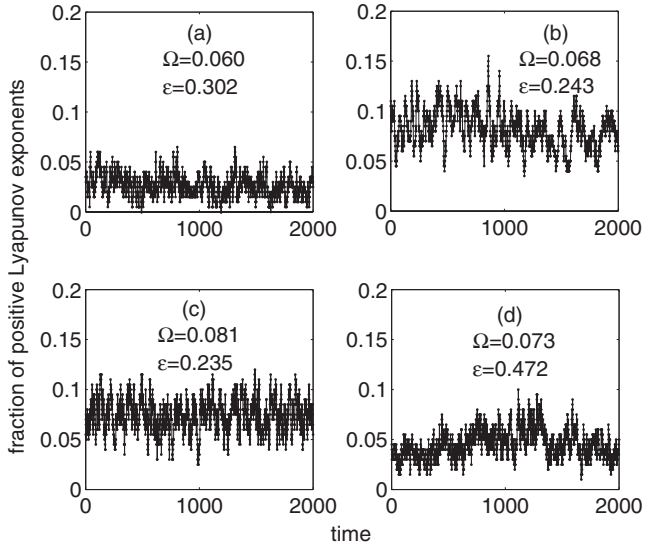

FIG. 6. The fraction of positive finite-time Lyapunov exponents (time = 20) as a function of t after the crisis. A transient of 200 000 iterates has been discarded with lattice size $L = 200$.

of expanding and contracting directions in phase space contributes to the existence of positive and negative Lyapunov exponents, respectively. The large time average over the infinite trajectory gives the asymptotic value of the Lyapunov exponents which ultimately determine the qualitative nature of the solution in the system. However, in the presence of nonhyperbolicity, the shadowing distance between the original chaotic orbits and the noisy ones diverges fast. Here, the determination of local expansion and contraction rates is more relevant than the asymptotic value, and is better quantified by the FTLEs, which average the local expansion and contraction rates and can be quantified for finite times. Thus, if a trajectory

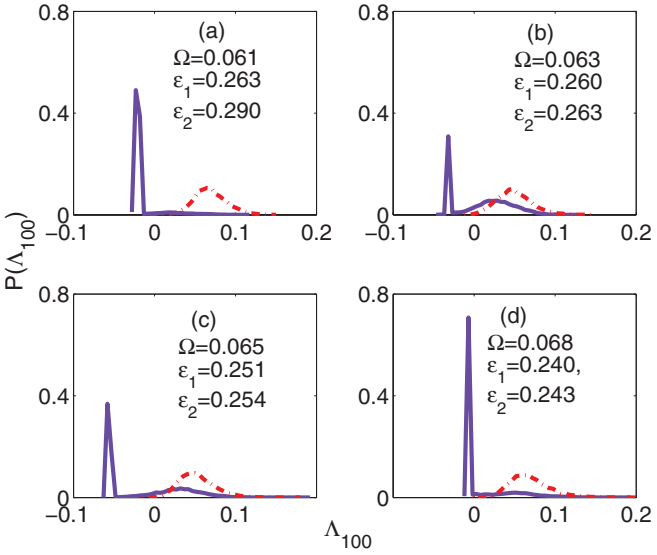

FIG. 7. (Color online) The probability distribution of largest finite-time (time = 100) Lyapunov exponent for precrisis ($\epsilon = \epsilon_1$, solid line) and postcrisis ($\epsilon = \epsilon_2$, dash-dottd line) parameter values. The data are collected for lattice size $L = 200$ over 10 000 time steps and averaging over 2 initial conditions.

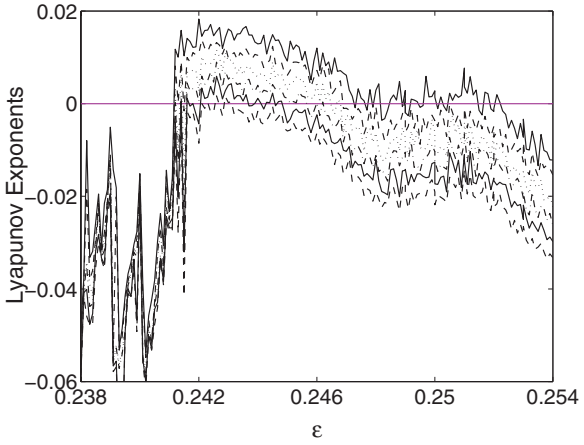

FIG. 8. (Color online) The six largest asymptotic Lyapunov exponents are plotted as a function of ϵ for $\Omega = 0.068$ with lattice size $L = 200$. Six Lyapunov exponents cross zero simultaneously just after the crisis. The maximum Lyapunov exponent starts oscillating about zero for $0.247 \leqslant \epsilon \leqslant 0.252$, showing the presence of UDV.

visits regions of the attractor having different numbers of expanding and contracting directions, the fraction of positive finite-time Lyapunov exponents will vary with time. We confirm the presence of UDV in our system by plotting the fraction of positive time-20 Lyapunov exponents for parameter values in the vicinity of the infection line after the crisis. The fraction of positive finite-time Lyapunov exponents as a function of time is plotted in Fig. 6 for four different parameter values, (a) $\Omega = 0.060$, $\epsilon = 0.302$, (b) $\Omega = 0.068$, $\epsilon = 0.243$, (c) $\Omega = 0.081$, $\epsilon = 0.235$, (d) $\Omega = 0.073$, $\epsilon = 0.472$. For all four cases we discard 400 000 transient iterations taking lattice size $N = 200$. It is clear that the fraction fluctuates, and that the trajectory visits regions with different numbers of stable and unstable directions. We note that these points are at different points along the infection line, so it is clear that the UDV is seen at all the points along the infection line.

The UDV is further illustrated in Fig. 7, which shows the distribution of the largest finite-time Lyapunov exponent

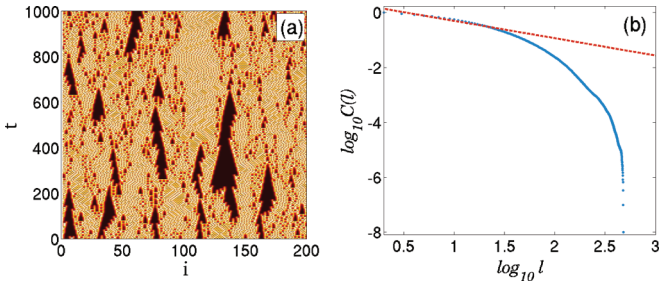

FIG. 9. (Color online) (a) The space-time plot of the spatiotemporally intermittent solution with 1000 iterates and lattice size $L = 200$ for $\Omega = 0.060$ and $\epsilon = 0.302$. A transient of 200 000 iterates has been discarded. (b) The log-log (base 10) plot of cumulative laminar length distribution for STI at $\Omega = 0.060$ and $\epsilon = 0.300$. The exponent ζ is 1.63 ± 0.05. The root-mean-square error for the fit up to laminar length $10^{1.5}$ is 0.04849 and the R^2 value is 0.9457. The data is taken for lattice size $L = 10\,000$ and averaging over 50 initial conditions. For each initial condition each lattice has been iterated for 50 000 iterates after discarding 50 000 iterates.

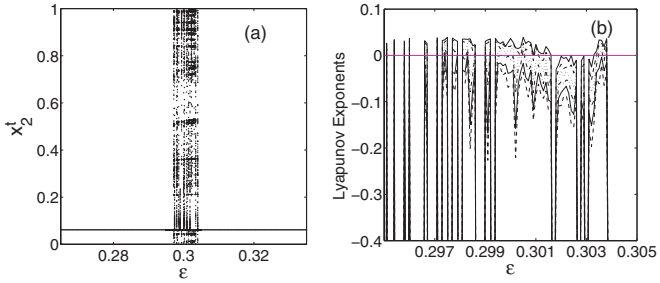

FIG. 10. (Color online) (a) The bifurcation diagram of the coupled map lattice at $\Omega = 0.060$ (marked by ◊ in Fig. 1). A typical site x_2^t is plotted over 200 time steps as function of the coupling strength ϵ in the neighborhood of the infection line, for lattice size $L = 200$. A transient of 50 000 iterates has been discarded. Synchronized solutions are seen before and after the crisis. (b) The six largest Lyapunov exponents are plotted as function of ϵ for $\Omega = 0.060$ for lattice size $L = 200$.

for different values of Ω and ϵ. We calculate the time-100 largest Lyapunov exponent taking lattice size $N = 200$ over 10 000 time steps and by averaging over 2 initial conditions. The distributions of the largest finite-time Lyapunov exponent before crisis are shown by solid lines, whereas the same quantities after crisis are shown by dotted lines. In the precrisis region the distributions are spread over positive and negative values with the peak at negative values. In contrast, the distributions shift towards the positive values only in a postcrisis situation. Unstable dimension variability is noticeable at this point and can be seen in the fluctuations of the largest Lyapunov exponent about zero in Fig. 8, plotted

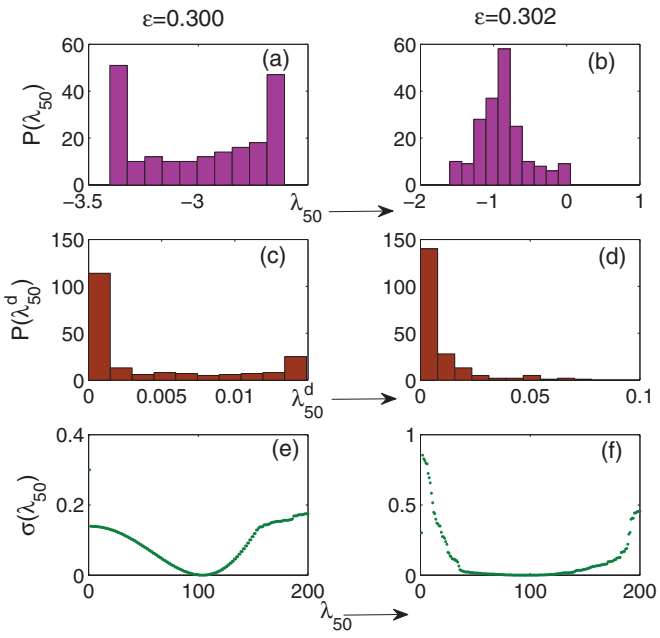

FIG. 11. (Color online) The distribution of time-50 Lyapunov exponents [(a), (b)], the difference between two consecutive time-50 Lyapunov exponents [(c), (d)], and the variance of time-50 Lyapunov exponents [(e), (f)] for $\Omega = 0.060$. The left and right columns correspond to the values of ϵ before and after crisis, respectively. The lattice size $L = 200$.

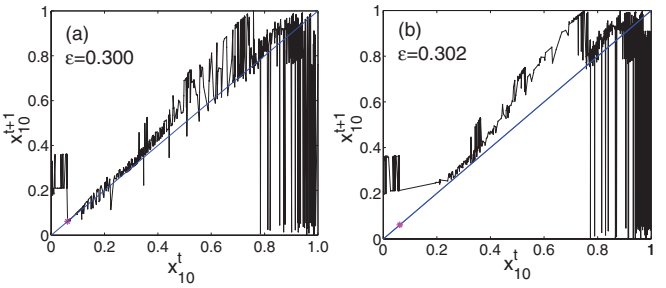

FIG. 12. (Color online) The site x_{10}^t is plotted with x_{10}^{t+1} for $\Omega = 0.060$ and (a) $\epsilon = 0.300$, (b) $\epsilon = 0.302$. In (a) the synchronized solution $x^* = 0.0615$ is stable. In (b) this solution becomes unstable via a tangent bifurcation.

for $\Omega = 0.068$. Similar fluctuations occur at other points along the infection line.

At the point under current discussion, the distribution of laminar lengths shows exponential behavior. However, as seen in earlier work, the system contains regions of spatiotemporal intermittency where the distribution of laminar lengths shows power-law behavior, with an exponent of the directed percolation class. We note that a full set of critical exponents, which characterize the order parameter, the susceptibility, and the correlation function, can be defined at these points, and turn out to belong to the directed percolation class [5]. These correspond to the parameter values at the edge of the synchronized regions in the spreading regime. Conversely, points on the edge of the synchronized regime in the nonspreading regime show spatially intermittent behavior with power-law behavior for the laminar length distributions, but with an exponent that does not belong to the directed percolation class. It is interesting to correlate the statistical characterizers seen here with the dynamical characterizers, and to identify the signatures of spatiotemporal behavior in both quantities. We discuss these in the next section.

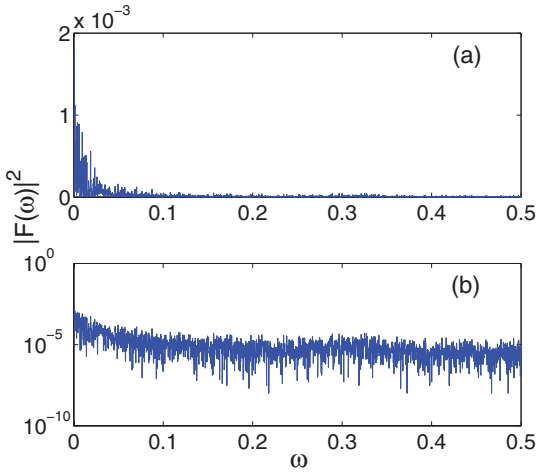

FIG. 13. (Color online) The power of the mode x_{101}^t has been plotted with frequency (a) linear scale (b) log scale for $\Omega = 0.073$ and $\epsilon = 0.472$. The signal shows chaos.

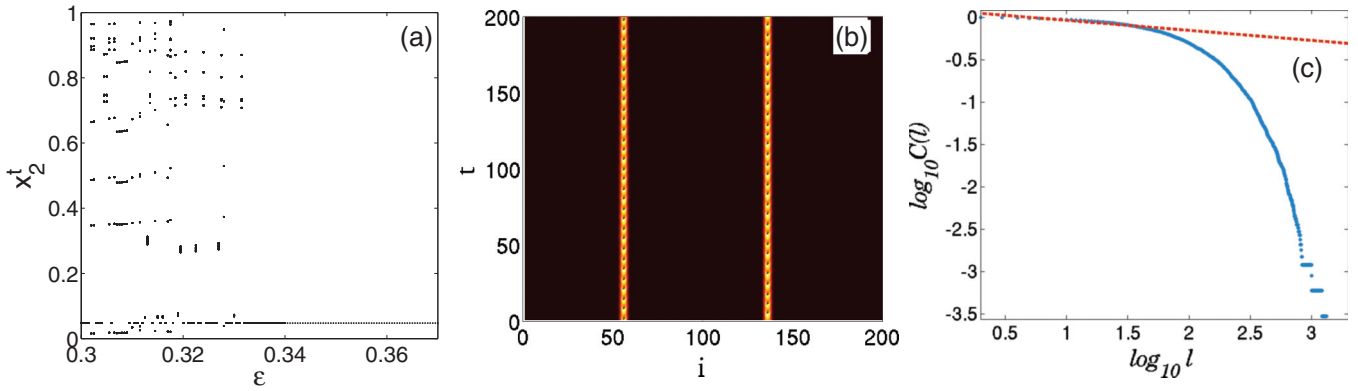

FIG. 14. (Color online) (a) The bifurcation diagram of the coupled map lattice at $\Omega = 0.040$ (marked by a ◯ in Fig. 1). A typical site x_2^t is plotted over 500 time steps as function of coupling strength ϵ in the neighborhood of the infection line, taking lattice size $L = 200$. A transient of 500 000 iterates has been discarded. (b) The space-time plot of an spatially intermittent solution with 1000 iterates and lattice size $L = 200$ for $\Omega = 0.040$ and $\epsilon = 0.402$. A transient of 200 000 iterates has been discarded. (c) The log-log (base 10) plot of the cumulative laminar length distribution at $\Omega = 0.040$ and $\epsilon = 0.402$. The exponent ζ is 1.1183 ± 0.0136. The root-mean-square error for the fit up to the laminar length $10^{1.7}$ is 0.01601 and the R^2 value is 0.8669. The data are taken for lattice size $L = 10\,000$ and averaged over 50 initial conditions. For each initial condition each lattice has been iterated for 50 000 iterates after discarding 50 000 iterates.

IV. SPATIOTEMPORAL AND SPATIAL INTERMITTENCY AND DYNAMICAL CHARACTERIZERS

We will illustrate the behavior seen at spatiotemporal intermittency at the left end of the infection line, the point marked with a diamond in the phase diagram (Fig. 1). Here the parameter values are $\Omega = 0.060$ and $\epsilon = 0.302$. We note that this point lies on the boundary of the synchronized solutions. A space-time plot of the solution is seen in Fig. 9(a). Spatiotemporally intermittent solutions can be clearly seen in the space-time plot. The distribution of laminar lengths shows power-law behavior with the exponent 1.63 ± 0.05 [see Fig. 9(b)]. The spatiotemporal intermittency seen here has been verified to belong to the directed percolation (DP) class [23]; hence the exponent is in agreement with the expected DP value.

The bifurcation diagram of a typical site can be seen in Fig. 10(a), and the Lyapunov exponents at the same value can be seen in Fig. 10(b). Synchronized solutions are seen above and below the infection line. An attractor widening solution is seen at the infection line. We plot a histogram of the time-50 finite-time Lyapunov exponents in Figs. 11(a) and 11(b). It is clear that the finite-time Lyapunov exponents are well below zero in the synchronized regime [Fig. 11(a)], and cross zero where the spreading modes are seen at $\epsilon = 0.302$ [Fig. 11(b)]. We also plot the histogram of the difference between consecutive values of the FTLEs in Figs. 11(c) and 11(d). Here, in the synchronized regime [Fig. 11(c)], the values are very closely clustered around zero, and the signature of the spreading mode is seen at crisis at $\epsilon = 0.302$ [Fig. 11(d)], where a gap in the spectrum is clearly seen. We also see a clear

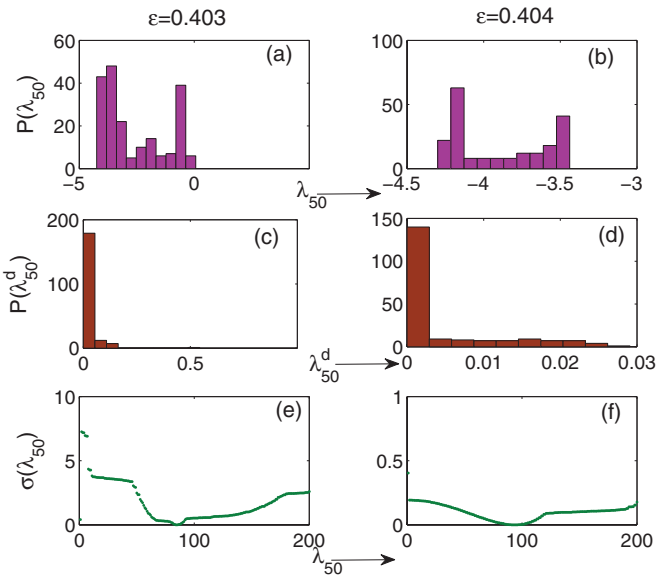

FIG. 15. (Color online) The distribution of time-50 Lyapunov exponents [(a), (b)], the difference between two consecutive time-50 Lyapunov exponents [(c), (d)], and the variance of time-50 Lyapunov exponents [(e), (f)] for $\Omega = 0.040$. The left and right columns correspond to the values of ϵ before and after crisis, respectively.

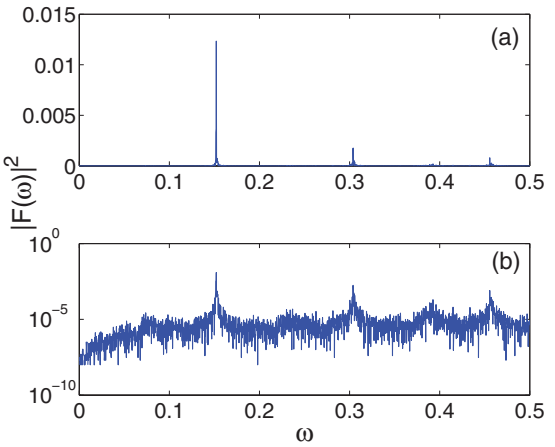

FIG. 16. (Color online) The power of the mode x_{56}^t has been plotted with frequency (a) linear scale and (b) log scale for $\Omega = 0.040$ and $\epsilon = 0.402$.

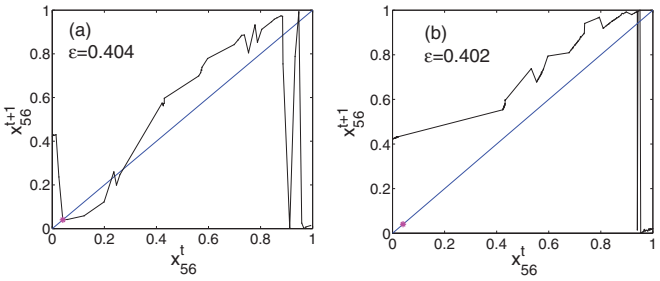

FIG. 17. (Color online) The site x^{t+1}_{56} is plotted with x^{t}_{56} for $\Omega = 0.040$ and for (a) $\epsilon = 0.404$, (b) $\epsilon = 0.402$.

signature in the variance of the FTLEs [see Figs. 11(e) and 11(f)]. The variance in the FTLEs is much broader after the crisis [Fig. 11(f)], and also shows discrete jumps reflective of the gaps in the distribution. The Lyapunov exponents of the system [Fig. 10(b)] show indications of unstable dimension variability, but they are not clear. However, the transition to spatiotemporal intermittency (STI) clearly takes place via a tangent bifurcation. This can be clearly seen in the plot of the return map of a typical site at the precritical and critical values of the parameter (see Fig. 12). It can be clearly seen that the fixed point of the map is barely stable at the critical value, but goes unstable beyond the critical value. Thus, the nonspreading to spreading transition is via a tangent bifurcation, as farther down the infection line, and corresponds to an attractor-widening crisis. (See Table V for the behaviour of the Floquet multipliers).

Similar behavior is seen at points along the boundary of the synchronized solutions that lie above the infection line, e.g., at the parameter values $\Omega = 0.073$ and $\epsilon = 0.472$, which is the point marked with a right triangle in the phase diagram (Fig. 1). The STI seen here belongs to the directed percolation class, the dynamical characterizers show similar behavior, and the power spectrum at a typical burst site (plotted in Fig. 13) shows clear chaotic behavior.

The intermittency seen at the edges of the synchronized solutions below the infection line belongs to a different universality class. Here, the bursts are noninfectious in nature, and spatial intermittency, where the distribution of laminar lengths scales as a power law, is seen. The laminar regions in this regime correspond to the synchronized solutions, although laminar regions could correspond to other kinds of dynamic regimes as well [25,29]. Similarly, the burst regimes can also correspond to different kinds of dynamics. In the regime considered here, the bursts in the spatially intermittent solutions can be periodic as well as quasiperiodic (see Fig. 1). Here, we discuss the behavior of the dynamic characterizers in these regimes.

A. Spatial intermittency with quasiperiodic bursts

These solutions are seen at the edges of the boundary of the synchronized solutions, below the infection line. We discuss the solutions at the parameter values marked with a circle in Fig. 1 ($\Omega = 0.040, \epsilon = 0.402$). The bifurcation diagram for a typical site and the space-time plot can be seen in Figs. 14(a) and 14(b), respectively. The distribution of laminar lengths shows power-law behavior with the power $\zeta = 1.1$ [Fig. 14(c)].

The distribution of the time-50 FTLEs shifts from the negative side seen for the synchronized solutions [Fig. 15(b)] to near zero values seen for the quasiperiodic bursts, Fig. 15(a). The difference between successive eigenvalues shows a much larger spread for the spatially intermittent solution [Fig. 15(d)], as compared with Fig. 15(c), and the variance of the FTLEs is smooth for the synchronized solution [Fig. 15(f)] and shows gaps for the spatially intermittent case Fig. 15(e). The power spectrum of a typical burst site demonstrates the quasiperiodic nature of the solution (Fig. 16). The synchronized solution goes unstable via a tangent bifurcation (Fig. 17).

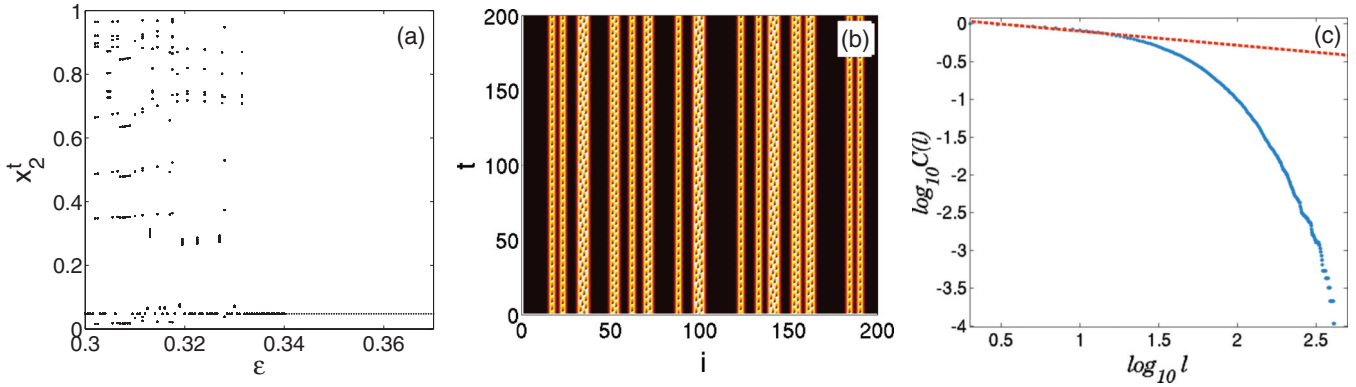

FIG. 18. (Color online) (a) The bifurcation diagram of the coupled map lattice at $\Omega = 0.047$ (marked by $\triangleleft$ in Fig. 1). The value of the variable at a typical site x^{t}_{2} is plotted over 500 time steps as function of the coupling strength ϵ in the neighborhood of the infection line, taking lattice size $L = 200$. A transient of 500 000 iterates has been discarded. A transition from a periodic solution to synchronized solution is observed at $\epsilon = 0.337$. (b) The space-time plot of the spatially intermittent solution with 1000 iterates and lattice size $L = 200$ for $\Omega = 0.047$ and $\epsilon = 0.32$. A transient of 200 000 iterates has been discarded. The period of the system is 5×13. (c) The log-log (base 10) plot of the cumulative laminar length distribution at $\Omega = 0.047$ and $\epsilon = 0.3360$. The exponent ζ is -1.1865 ± 0.0284. The root-mean-square error for fit up to laminar length $10^{1.3}$ is 0.01562 and the R^2 value is 0.9237. The data are taken for lattice size $L = 10\,000$ and averaging over 50 initial conditions. For each initial condition the lattice has been iterated for 50 000 iterates after discarding 50 000 iterates.

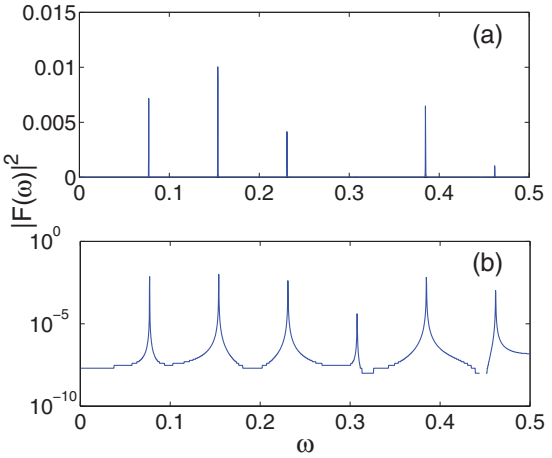

FIG. 19. (Color online) The power of the mode x^t_{101} has been plotted with frequency (a) linear scale and (b) log scale for $\Omega = 0.047$ and $\epsilon = 0.320$. The signal shows frequencies at 0.077,0.154,0.231,0.308,0.385,0.462. The period of the mode x_{101} is 13. The period of the full system is 5×13.

B. Spatial intermittency with periodic bursts

Spatial intermittency with periodic bursts is also seen below the infection line. We discuss the dynamical behavior at the point marked with a left triangle on the phase diagram (Fig. 1), i.e., at the parameter values ($\Omega = 0.047, \epsilon = 0.3360$). Here, the periodic bursts have time period 5. The bifurcation diagram at a burst site can be seen in Fig. 18(a). The space-time plot of the solution can be seen in Fig. 18(b). The distribution of laminar lengths scales as a power law with exponent $\zeta = 1.18$ [Fig. 18(c)]. The power spectrum of a burst site is seen in Fig. 19. The Floquet multipliers (Table VI) and the return map (Fig. 20) indicate that the spatially intermittent period-5 state is obtained by a bifurcation from a synchronized solution. The distribution of FTLEs (Fig. 21) shifts from a completely negative range for the synchronized solution [Fig. 21(a)] to an upper bound in the vicinity of zero for the period-5 intermittent solution [Fig. 21(b)]. The histogram of the difference between consecutive values of the FTLEs [Fig. 21(d)] shows wide spreads for the spatially intermittent solution, and a far narrower spread for the synchronized (and laminar) solution [Fig. 21(c)]. The signature of each kind of solution is also seen in the distribution of variances and is smooth for the synchronized case [Fig. 21(e)] and discontinuous for the spatially intermittent case [Fig. 21(f)].

TABLE VI. Floquet multipliers at $\Omega = 0.047$ starting from one randomly chosen initial condition after discarding 210 000 iterates for lattice size $L = 200$.

ϵ	Nature of solution	Number of Floquet multipliers more than 1
0.335	time periodic with period 5	0 (5-time Floquet multiplier), 2 (1-time Floquet multiplier)
0.336	time periodic with period 5	0 (5-time Floquet multiplier), 4 (1-time Floquet multiplier)
0.337	synchronized	0 (5-time), 0 (1-time)
0.338	synchronized	0 (5-time), 0 (1-time)

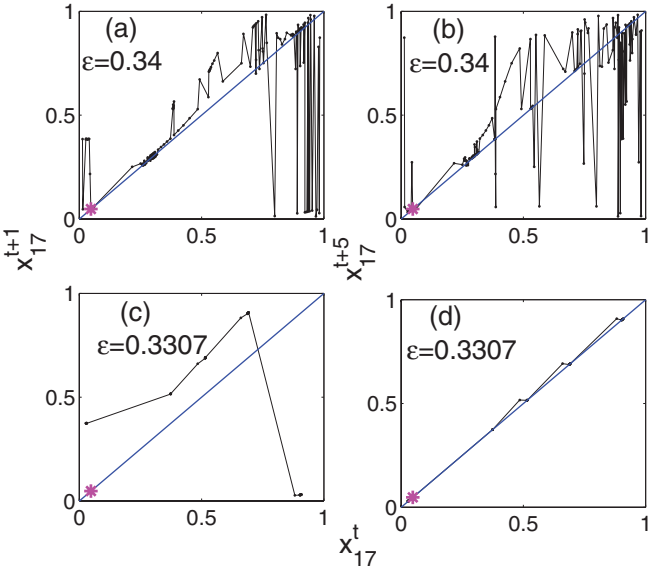

FIG. 20. (Color online) The site x^t_{17} is plotted with x^{t+1}_{17} (left column) and with x^{t+5}_{17} (right column) for $\Omega = 0.047$. For $\epsilon = 0.34$ synchronized solution is stable, whereas for $\epsilon = 0.3307$ the time periodic solution with temporal period-5 is stable.

Thus, in the case of spatial and spatiotemporal intermittency, the dynamic characterizers provide a detailed characterization of the type of solution seen before the bifurcation and can identify the type of bifurcation, as well as the critical value of the parameter where the bifurcation takes place. The present analysis is for a situation where the laminar state is the synchronized state, but can be straightforwardly extended to situations where the laminar state is of other

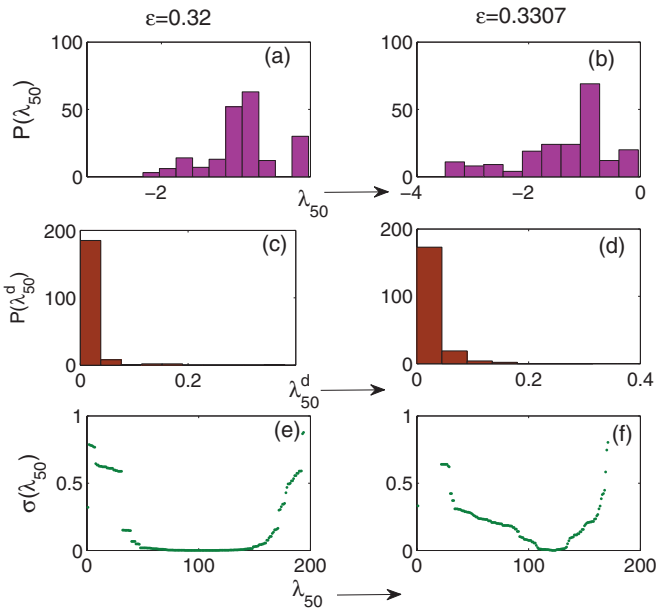

FIG. 21. (Color online) The distribution of time-50 Lyapunov exponents [(a), (b)], the difference between two consecutive time-50 Lyapunov exponents [(c), (d)], and the variance of time-50 Lyapunov exponents for $\Omega = 0.040$. The left and right columns correspond to the values of ϵ before and after crisis, respectively.

types, e.g., of higher periods [29], or of the traveling wave type [22,25,30]. The characterizers are simple and can be easily constructed for the broad variety of systems that show spatiotemporal intermittency [14–20,31]. Spatial analogs and statistical quantities can further classify the patterns.

V. SUMMARY AND CONCLUSIONS

To summarize, we study the phenomenon of crisis and its consequences in a system with a high-dimensional phase space. The attractor widening crisis in this dynamical system translates to a spreading transition in the phase diagram of the system. Spreading modes can be clearly seen in the space-time plots of the system post crisis, and the corresponding attractor widening can be seen in the bifurcation diagram. Thus the spreading transition has its dynamical origins in an attractor widening crisis. The signatures of the spreading and nonspreading modes can be seen in the statistical characterizers, and the signatures of the dynamical behavior of the modes can be seen in the dynamical characterizers. The high-dimensionality of the phase space of the system contributes special features to the crisis, including strong unstable dimension variability at the infection line, and the existence of multiple routes to crisis, depending on the initial conditions. We list some of the multiple routes seen here, in this paper. Multiattractor systems with fractal basins of attraction have been seen earlier in the context of food chains, and it is possible that phenomena of the kind seen here appear in such systems.

We identify the nature of the bifurcation that gives rise to the crisis. Although there are multiple routes to crisis, the Floquet multipliers of the system and return maps indicate that the crisis occurs due to tangent bifurcations in every case studied. The signatures of the unstable dimension variability near the crisis are seen in the fluctuations in the number of positive eigenvalues and fluctuations in the largest Lyapunov exponents around zero. The signatures are strong around the middle of the infection line and less strong about the edges.

We also set up additional dynamical characterizers, viz. distributions of finite-time Lyapunov exponents, statistics of level separations (i.e., differences between successive FTLEs), and variances of FTLEs [31]. These also contain strong signatures of the dynamical behaviors of the system pre- and postcrisis. We note that fields of FTLEs have been used as identifiers of Lagrangian coherent structures in a variety of contexts ranging from fluid flows [32] to urban transport [33]. It would be interesting to see whether the dynamical characterizers used in the present paper, viz. the distributions of FTLEs, level separations, and variances, are able to yield useful information in these and other contexts.

Finally, special solutions of the spreading and nonspreading types are seen at the boundaries of the synchronized solution. The special solutions of the spreading or infecting type, seen above the infection line, are spatiotemporally intermittent in nature, whereas the nonspreading solutions or noninfecting solutions seen below the infection line are spatially intermittent in nature. Statistical characterizers are essential to characterize the difference between the two kinds of solutions. The spatiotemporally intermittent, infecting solutions show scaling behavior and a complete set of directed percolation exponents [5,23], and belong to the DP universality class, whereas the noninfecting solutions show scaling behavior and an exponent characteristic of spatial intermittency, which does not belong to the DP class. Thus, the statistical characterization is essential to identify the universality class of the system.

The dynamical characterization can identify the type of bifurcation that takes place, as well as the dynamical nature of the spreading and nonspreading modes. Power spectra are useful to identify the exact dynamics of the burst states. We also note here that the origin of the emergence of two distinct universality classes for the same system lies in a dynamical phenomenon, viz. the crisis which occurs at the infection line. Thus the dynamical and statistical phenomena are linked at a fundamental level. Hence, both statistical and dynamical characterizations are required for the complete understanding of the behavior of the system.

We also note that that the cellular automaton version of the system shows a transition from a deterministic cellular automaton to a probabilistic cellular automaton at the crisis line [5]. Thus the phenomena are linked at three levels, the transition in the cellular automaton, the spreading transition in the space-time plots, and the crisis in the dynamical system. We also intend to see whether the cellular automaton level of description can provide further insights into the system.

Thus, the spatiotemporal dynamics of extended systems has implications for their statistical behavior. Our analysis indicates that both dynamical and statistical characterizers complement each other in the analysis of the spatiotemporal dynamics of extended systems. In most studies of pattern formation, e.g., sand pile problems and cellular automata, statistical characterization is used to understand the behavior of the system. The present study indicates that a twofold characterization is necessary for the complete analysis of evolving extended systems. Some of the characterizers discussed here can go some way towards this. The development of further tools for the analysis of evolving systems with many degrees of freedom is also important. We hope this work will provide some impetus towards this.

[1] E. Ott, *Chaos in Dynamical Systems* (Cambridge University Press, Cambridge, UK, 2002).

[2] C. Grebogi, E. Ott, F. Romeiras, and J. A. Yorke, Physica D **7**, 181 (1993).

[3] A. E. Motter, Y. C. Lai, and C. Grebogi, Phys. Rev. E **68**, 056307 (2003); G. T. Kubo, R. L. Viana, S. R. Lopes, and C. Grebogi, Phys. Lett. A **34**, 5569 (2008).

[4] N. N. Thyagu and N. Gupte, Phys. Rev. E **76**, 046218 (2007); Pramana **70**, 1031 (2008).

[5] Z. Jabeen and N. Gupte, Phys. Lett. A **374**, 4488 (2010).

[6] R. K. Upadhyay, Chaos Solitons Fractals **16**, 737 (2003).

[7] M. P. Boer, B. W. Kooi, and S. A. L. M. Kooijman, Math. Biosci. **169**, 109 (2001).

[8] F. Daviaud, J. Lega, P. Berge, P. Coullet, and M. Dubois, Physica D **55**, 287 (1992).
[9] R. Kapral and K. Showalter, *Chemical Waves and Patterns* (Kluwer Academic Publishers, Dordrecht, Netherlands, 1995).
[10] H. Chate and P. Manneville, Physica A **224**, 348 (1996).
[11] P. K. Maini, K. J. Painter, and H. N. P. Chau, J. Chem. Soc. Faraday Trans. **93**, 3601 (1997).
[12] F. X. Witkowski, L. J. Leon, P. A. Penkose, W. R. Giles, M. L. Spano, W. L. Ditto, and A. T. Winfree, Nature (London) **392**, 78 (1998).
[13] P. S. Marcus, Annu. Rev. Astron. Astrophys. **31**, 523 (1993).
[14] R. Kapral, in *Theory and Applications of Coupled Map Lattices*, edited by K. Kaneko (Wiley, New York, 1993), Chap. 5, p. 135.
[15] F. Daviaud, M. Dubois, and P. Berge, Europhys. Lett. **9**, 441 (1989); S. Ciliberto and P. Bigazzi, Phys. Rev. Lett. **60**, 286 (1988).
[16] S. Bottin, F. Daviaud, O. Dauchot, and P. Manneville, Europhys. Lett. **43**, 171 (1998); P. W. Colovas and C. D. Andereck, Phys. Rev. E **55**, 2736 (1997); A. Goharzadeh and I. Mutabazi, Eur. Phys. J. B **19**, 157 (2001).
[17] *Theory and Applications of Coupled Map Lattices*, edited by K. Kaneko (Wiley, New York, 1993) Ref. [9], and references therein; J. Rolf, T. Bohr, and M. H. Jensen, Phys. Rev. E **57**, R2503 (1998); H. Chate and P. Manneville, Physica D **32**, 409 (1988); C. I. Christov and G. Nicolis, Physica A **228**, 326 (1996); *Dynamical Systems Approach to Turbulence*, edited by T. Bohr, M. H. Jensen, G. Paladin, and A. Vulpiani (Cambridge University Press, Cambridge, 1998).
[18] H. Chate, Nonlinearity **7**, 185 (1994); M. G. Zimmermann, R. Toral, O. Piro, and M. San Miguel, Phys. Rev. Lett. **85**, 3612 (2000).
[19] G. V. Osipov, M. V. Ivanchenko, J. Kurths, and B. Hu, Phys. Rev. E **71**, 056209 (2005).
[20] M. Cross and H. Greenside, *Pattern Formation and Dynamics in Nonequilibrium Systems* (Cambridge University Press, Cambridge, UK, 2009).
[21] The phase diagram shows solutions of other periods as well. Some of these can be seen in Refs. [5,22].
[22] Z. Jabeen and N. Gupte, Phys. Rev. E **74**, 016210 (2006).
[23] Z. Jabeen and N. Gupte, Physica A **384**, 59 (2007).
[24] T. M. Janaki, S. Sinha, and N. Gupte, Phys. Rev. E **67**, 056218 (2003).
[25] Z. Jabeen and N. Gupte, Phys. Rev. E **72**, 016202 (2005).
[26] J. Milnor, Commun. Math. Phys. **99**, 177 (1985); **102**, 517 (1985).
[27] We note that our calculations have been carried out for lattice sizes $L = 50$, $L = 100$, $L = 200$. In the case of the multiple routes to crisis, the routes differ for $L = 50$ and $L = 200$. However, the last period before the crisis is the same in both cases. We have quoted the route for $L = 50$ for $\Omega = 0.065$ and $L = 200$ for $\Omega = 0.068$.
[28] In the case of the distributions of finite time Lyapunov exponents, these have been calculated for the lattice sizes $L = 50$ and $L = 200$. The distributions shown in the paper are for $L = 200$. There is no change in the qualitative features as described in the paper. Thus we conclude that features which show initial condition dependence such as the multiple routes to crisis are also sensitive to lattice size, at least at lattice sizes of order 100, whereas features which are statistical in nature such as distributions of FTLEs do not depend on the size, even at this level.
[29] A. Sharma and N. Gupte, Phys. Rev. E **66**, 036210 (2002).
[30] In the case of other kinds of laminar states, the transition may take place via other types of bifurcations; e.g., for a traveling wave base state, a tangent period doubling bifurcation takes the sine circle map system to spatiotemporal intermittency [22].
[31] K. A. Takeuchi, H. Chate, F. Ginelli, A. Politi, and A. Torcini, Phys. Rev. Lett. **107**, 124101 (2011).
[32] G. Haller, Physica D **149**, 248 (2001).
[33] W. Tang, B. Knutson, A. Mahalov, and R. Dimitrova, Phys. Fluids **24**, 063302 (2012).